IOP PUBLISHING PLASMA PHYSICS AND CONTROLLED FUSION

Plasma Phys. Control. Fusion **49** (2007) A109–A119 doi:10.1088/0741-3335/49/5A/S09

Numerical simulations of collisional drift-wave turbulence in a magnetized plasma column

C Holland, G R Tynan, J H Yu A James, D Nishijima, M Shimada and N Taheri

Department of Mechanical and Aerospace Engineering, University of California, San Diego, La Jolla, CA 92093, USA

Received 31 May 2006, in final form 17 October 2006
Published 28 March 2007
Online at stacks.iop.org/PPCF/49/A109

Abstract

Zonal flows are known to be a key player in the regulation of drift-wave turbulence and have been observed in a wide variety of plasma devices. Current attempts to describe the formation and dynamics of zonal flows and drift-waves in a simple magnetized column via numerical simulation of the Hasegawa–Wakatani model are described here. The simulations are shown to exhibit the formation of a zonal flow whose profile is well-predicted by analytic theory and in qualitative agreement with experimental observations. However, the magnitude of the zonal flow and fluctuation levels appear to be significantly overestimated by the simulation. Details of the numerical model and sensitivity to initial conditions are also described.

(Some figures in this article are in colour only in the electronic version)

1. Introduction

In magnetic confinement based fusion energy devices, drift-wave turbulence and its associated transport are believed to provide the main limitation on plasma performance, in the absence of MHD or other large-scale plasma instabilities. Drift-waves are small-scale ($l \sim \rho_i$, where $\rho_i = V_{Ti}/\Omega_{ci}$ is the ion gyroradius), slow ($\omega \sim C_s/L$, where $C_s = \sqrt{T_e/M_i}$ is the sound speed and L is a typical scale length of the equilibrium profiles) quasi-neutral fluctuations driven by the inherent density and temperature gradients of the plasma [1]. Extensive analytic and numerical analysis in the last decade has shown that drift-wave turbulence is regulated by zonal flows—axisymmetric, radially sheared $\vec{E} \times \vec{B}$ flows [2]. Because these zonal flows are axisymmetric, they have no radial velocity associated with them ($V_r = cE_\theta/B \propto \partial_\theta \phi = 0$), and so they cannot extract energy from the background gradients and are therefore linearly stable. However, they can be generated nonlinearly via the turbulent Reynolds stress [3] and will then in turn saturate the turbulence via radially shearing and decorrelating the eddies [4]. Experimental observations of this predicted 'drift-wave–zonal flow' paradigm have somewhat lagged the theoretical predictions, but a number of machines have now reported on observations

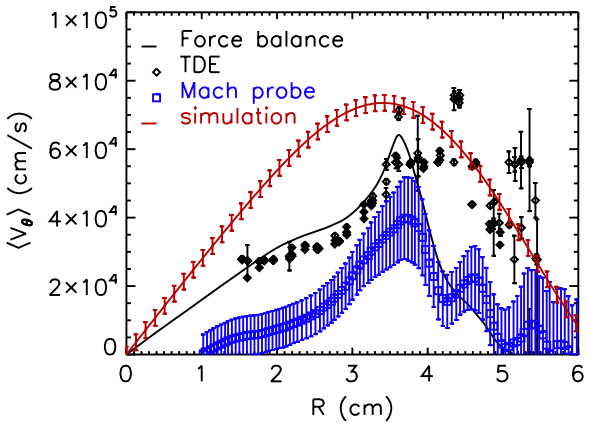

Figure 1. Experimentally measured profiles of the mean azimuthal velocity in CSDX, obtained via solving the azimuthal momentum equation using the experimentally measured Reynolds stress profile, TDE analysis of Langmuir probe data and Mach probe measurements. The time-averaged zonal velocity from simulation is also shown.

of zonal flows and their interactions with turbulence [5–10]. Representative papers describing current experimental results can be found in [11], while a recent review paper by Diamond *et al* surveys the state of analytic and computational results (in addition to experimental observations) [12].

Experimental studies of zonal flows in high-power confinement devices are generally quite difficult due to limited fluctuation diagnostic access inside the last closed flux surface, particularly for observations of spatially resolved electric field or electrostatic potential fluctuations needed to directly measure the zonal flows. However, the process of zonal flow generation is believed to be a fairly universal property of magnetized plasmas, as a sufficiently strong magnetic field ensures that the turbulent dynamics are essentially two-dimensional, leading to an 'inverse cascade' of kinetic energy believed to be responsible for the formation of the zonal flows, analogous to the dynamics of two-dimensional neutral fluids [13]. Leveraging this fact, the (C)ontrolled (S)hear (D)ecorrelation E(x)periment (CSDX) has been constructed to study drift-wave and zonal flow dynamics in a simple experimental realization. CSDX is a low-temperature ($T_e \leqslant 3.5$ eV, $T_i \approx 0.5$–1 eV) helicon plasma column with an axial magnetic field, which exhibits a controlled transition to broadband drift-wave turbulence as the magnetic field is increased from 400 to 1000 G; a thorough summary of the machine can be found in [14].

Previous publications [14–17] have focused on characterization of CSDX plasmas, most recently demonstrating that there is a poloidally symmetric radially sheared flow (e.g. a zonal flow) nonlinearly generated by the turbulence via consideration of the azimuthal momentum equation [16, 17]. Experimental measurements of the Reynolds stress were combined with estimated linear damping rates to solve for a self-consistent mean azimuthal velocity, which was shown to be in agreement with measurements of the flow profile obtained via time-delay estimation (TDE) [18] (i.e. cross-correlation of spatially separated measurements) and Mach probe measurements; the results are shown in figure 1. The observed flow profile was also found to be in qualitative agreement with the zonal flow profile predicted via numerical simulation. In this paper we present a more detailed characterization of this numerical simulation, detailing the algorithm used, and a more complete discussion of the previously published results. We then describe new results which document the existence of multiple possible nonlinear endstates.

Both sets of results are compared against experimentally measured fluctuation profiles, with limited agreement in either case, motivating a brief discussion of potential extensions to the numerical model which may allow for more accurate reproduction of the experimental results.

2. Model overview

The simplest self-consistent model of collisional drift-wave turbulence which includes both linear instability and a turbulent flux was first given by Hasegawa and Wakatani [19], and describes the coupled evolution of density and vorticity under the assumptions of uniform electron temperature and cold ions; it is this model which is used in our simulations. The governing equations can be written in dimensionless form as

$$\frac{\partial n}{\partial t} + \vec{V} \cdot \vec{\nabla}\, n + \frac{V^*}{r}\frac{\partial \phi}{\partial \theta} + \omega_{\|}(n-\phi) = D\nabla_{\perp}^2 n, \tag{1}$$

$$\frac{\partial \nabla_{\perp}^2 \phi}{\partial t} + (\vec{V} \cdot \vec{\nabla})\nabla_{\perp}^2 \phi + \omega_{\|}(n-\phi) + \nu_{\mathrm{i-n}}\nabla_{\perp}^2 \phi = \mu_{\mathrm{ii}}\nabla_{\perp}^4 \phi, \tag{2}$$

where $\vec{V} = -\vec{\nabla}\,\phi \times \hat{z}$. The spatial scales have been normalized by $\rho_{\mathrm{s}} = C_{\mathrm{s}}/\Omega_{\mathrm{ci}}$, where $C_{\mathrm{s}} = \sqrt{T_{\mathrm{e}}/M}$ is the ion acoustic speed and Ω_{ci} is the ion gyrofrequency, and the time scales have been normalized by $C_{\mathrm{s}}/L_{\mathrm{n}}$, where L_{n} is the density gradient scale length. The field quantities are 'mixing-length normalized' and are given by $n = (L_{\mathrm{n}}/\rho_{\mathrm{s}})(\tilde{\mathrm{n}}/\langle n \rangle)$ and $\phi = (L_{\mathrm{n}}/\rho_{\mathrm{s}})((e\tilde{\phi})/T_{\mathrm{e}})$. In addition, $V^* = -\rho_{\mathrm{s}} C_{\mathrm{S}} \mathrm{d}\ln n_0/\mathrm{d}r$ is the (electron) diamagnetic velocity, V_{Te} is the electron thermal speed and $\mu_{\mathrm{ii}} = 0.3\rho_{\mathrm{i}}^2 \upsilon_{\mathrm{ii}}$ is the ion viscosity. The effects of parallel electron collisionality (i.e. resistivity) are described by $\omega_{\|} \equiv k_{\|}^2 V_{\mathrm{Te}}^2/\upsilon_{\mathrm{e}}$ (where υ_{e} is the electron collision frequency). The magnitude of this parameter quantifies the degree to which the Boltzmann relation $n_{\mathrm{e}} = n_0 \exp(-e\phi/k_{\mathrm{B}}T_{\mathrm{e}})$ (and thereby $n = \phi$) is maintained via parallel electron dynamics: large values of $\omega_{\|}$ (corresponding to weak collisionality) force n and ϕ to be essentially equal, such that as $\omega_{\|} \to \infty$, $n \to \phi$ and the model reduces to the one-field Hasegawa–Mima system [20]. In the case of $\omega_{\|} \to 0$, the system reduces to the advection of a passive scalar with a mean gradient (the density) by the flow field of a two-dimensional incompressible flow (i.e. equation (2) reduces to the Euler equation). The effects of flow drag due to ion–neutral collisions is represented by the $\nu_{\mathrm{i-n}}$ term (where the neutrals are assumed to have negligible velocities) [21]. Note that this dissipation has a form that is identical to flow damping that occurs in toroidal systems due to magnetic pumping and neoclassical viscosity [22] which can be an important component of the dynamics of the shear layer which forms just inside the magnetic separatrix in high-power confinment devices at the L–H transition [23]. However, in our low-temperature plasma, the ion viscosity is roughly an order of magnitude larger than this term.

We have developed an initial-value simulation for comparison with our experimental results, which evolves the model described above in the cylindrical geometry of our experiment from an initial field of spatially uniform small-amplitude white noise. The code is two-dimensional (i.e. is in r–θ space) and treats the poloidal direction spectrally (using a one-third rule to prevent aliasing) while radial derivatives are found using 3-point finite differencing in order to retain the full cylindrical geometry of the experiment. Finite m fluctuations are all assumed to have a single value of $\omega_{\|}$ (equivalent to a single parallel wavenumber), while the $m = 0$ potential fluctuation is taken to have $k_{\|} = 0$ (and so $\omega_{\|} = 0$ for these fluctuations). The finite m mode amplitudes go to zero at $r = 0$ and $r = a$ (where a is the radius of the cylinder), while the $m = 0$ potential fluctuation amplitude vanishes at $r = a$ and $\partial\phi_{m=0}/\partial r = 0$ at $r = 0$. To mimic the effects of ionization sources which maintain the

equilibrium density profile and prevent quasilinear flattening, the $m = 0$ density fluctuation term is not evolved so that the overall $m = 0$ density component is simply the imposed equilibrium density $\langle n \rangle = n_0 \exp(-0.5r^2/L_n^2)$ (which gives a constant diamagnetic frequency $\omega^* = -m(\rho_s C_s)/r)(\mathrm{d}\ln\langle n\rangle)/\mathrm{d}r) = m(\rho_s C_s)/L_n^2$). Note that with this equilibrium density profile, it is straightforward to show that the eigenfunctions of the system are the Bessel functions $J_m(k_\perp r)$, which allows for analytic expressions of the perpendicular wavenumbers in terms of the zeros of the Bessel functions (i.e. the nth wavenumber is given by $k_\perp = X_{mn}/a$, where X_{mn} is the nth zero of the mth Bessel function), and solution of the linear dispersion relation follows directly. The equations are integrated by a split implicit/explicit scheme, where the left-hand sides of equations (1) and (2) are first integrated by a second-order Runge–Kutta (leapfrog) scheme (with the nonlinear convolutions calculated in real space using the Arakawa discretization scheme [24]), and then the dissipative terms on the right-hand side are solved implicitly. More specifically, equations (1) and (2) can be rewritten as (with $\Omega = \nabla_\perp^2 \phi$)

$$(\partial_t - D\nabla_\perp^2)n = f_n(n, \phi), \tag{3}$$

$$(\partial_t - \mu_{ii}\nabla_\perp^2)\Omega = f_\Omega(n, \phi, \Omega). \tag{4}$$

The solution for the density at $t + \Delta t$ is then given by $(1 - \Delta t D\nabla_{ij}^2)n_{i,j}^{t+\Delta t} = n_{i,j}^t + \hat{f}_n$, where $\hat{f}_n = \int_t^{t+\Delta t} \mathrm{d}t' f_n$ calculated via the leapfrog scheme and ∇_{ij}^2 is the discretized Laplacian operator; the vorticity equation is iterated in an analogous manner.

3. Simulation results

The results previously published in [16] used 64 points in the radial direction and 128 azimuthal points (giving 42 meaningful poloidal modes) and in normalized units, $\omega_\parallel = 1$, $D = 0.05$, $\nu_{i-n} = 0.03$, $\mu_{ii} = 0.4$, $\rho_s = 1$ cm, $L_n = 2$ cm and $a = 8$ cm (corresponding to the parameters used in the momentum balance analysis discussed in [16, 17], since $C_s = 2 \times 10^5\,\mathrm{cm\,s^{-1}}$ for the conditions of these experiments, although a constant value of μ_{ii} is used here, instead of the radially varying profile used in the momentum balance analysis). This corresponds to $\Delta r = 0.125$ cm, $\Delta\theta = 0.05$; a timestep of $\Delta t = 5 \times 10^{-3}\, L_n/C_s = 5 \times 10^{-8}$ s was used. The initial conditions are such that at each radial location (other than $r = 0$ and $r = a$) potential and density fluctuations with finite poloidal mode numbers m are initialized as small-amplitude white noise (constant amplitude, but randomly distributed phases for each value of $\phi(r, m)$ and $n(r, m)$); the zonal ($m = 0$) potential fluctuation is set to zero at $t = 0$. Figure 2 shows the analytically calculated linear growth rate for the longest radial wavelength modes as a function of poloidal mode number m (which are the only unstable modes), illustrating only poloidal mode numbers $m = 2$–5 are linearly unstable. The overall energetics of the system can be described by combining equations (1) and (2) to write

$$\frac{\mathrm{d}E_{tot}}{\mathrm{d}t} = \Gamma - \omega_\parallel\langle(n - \phi - \phi_{ZF})^2\rangle - D\left\langle|\nabla_\perp n|^2\right\rangle - \upsilon_{i-n}\langle|\nabla_\perp\phi|^2\rangle - \mu_{ii}\langle|\nabla_\perp^2\phi|^2\rangle, \tag{5}$$

where $E_{tot} = \frac{1}{2}, (\langle n^2\rangle + \langle|\nabla_\perp\phi|^2\rangle)$, $\Gamma = -(\rho_s/L_n)\langle(n/r)(\partial\phi/\partial\theta)\rangle$, $\phi_{ZF} = (1/(2\pi))\int_0^{2\pi}\mathrm{d}\theta\phi$ is the $m = 0$ component of the potential and $\langle f\rangle = (1/\pi a^2)\int_0^{2\pi}\int_0^a r\mathrm{d}r\mathrm{d}\theta f$. Figure 3 shows the time history of E_{tot} and the various terms of equation (5), as well as the error $\varepsilon = \mathrm{d}_t E_{tot} - \Gamma + \omega_\parallel\langle(n - \phi - \phi_{ZF})^2\rangle + D\langle|\nabla_\perp n|^2\rangle + \upsilon_{i-n}\langle|\nabla_\perp\phi|^2\rangle + \mu_{ii}\langle|\nabla_\perp^2\phi|^2\rangle$. The error is significantly smaller than all the terms in the global energy balance, demonstrating that energy is extremely well-conserved. Note that the diffusion term in equation (1) is introduced for purely numerical reasons, in order to damp small-scale density fluctuations generated by $\vec{E} \times \vec{B}$ convection; as the value of D used is an order of magnitude smaller than the (physical)

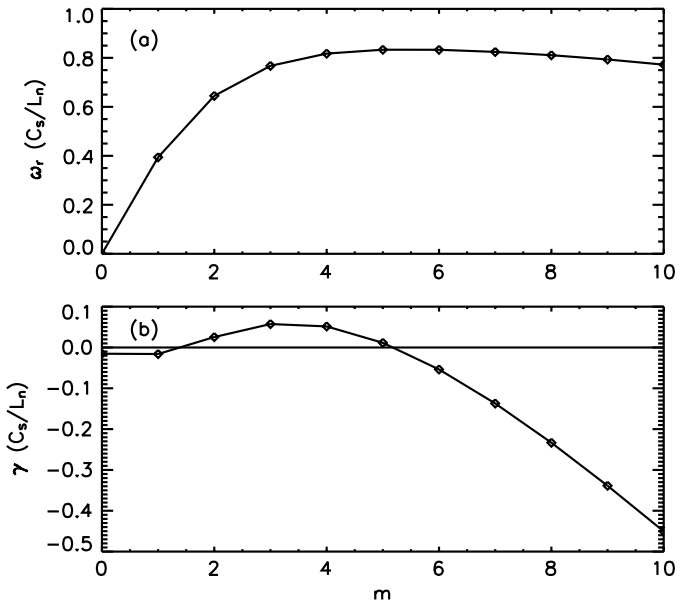

Figure 2. Linear frequency and growth rate for longest radial wavelength modes.

μ_{ii}, it has only a minor effect on the linear growth rate or nonlinear dynamics (where parallel dissipation and viscosity are stronger energy sinks, shown in figure 3(*b*).

The dominant feature of these simulations is that after the initial linear growth phase ($t \leqslant 100\ L_n/C_s$) a limit cycle behaviour emerges, with the system alternating between strong zonal flow (defined as the $m = 0$ potential fluctuation) and weak finite m modes and strong finite m modes with weak zonal flow. Snapshots of the density and potential from different representative times are shown in figure 4, which illustrate that the dynamics of the system are dominated by the $m = 3$ mode and the zonal flow. This limit cycle behaviour can be seen as one extreme of the predator–prey type behaviour coupled drift-wave–zonal flow systems are predicted to exhibit analytically [25]. However, most numerical simulations of drift-wave turbulence (either of collisionally destabilized modes such as those described here or collisionless temperature gradient driven modes) have not exhibited such a dramatic or clear limit cycle as what is observed here, tending rather to reach a well-defined or slowly evolving saturated state, with varying levels of intermittency or 'burstiness' [12].

Additional simulations (using the same physical and numerical parameters) have revealed the existence of a second nonlinear state, in which the fluctuation amplitudes do settle into steady values. A time trace of the total energy along with the conservation properties for this case is shown in figure 5, with snapshots of the potential and density fluctuations in the saturated state shown in figure 6. A particularly intriguing feature of both cases is that the profile of the mean zonal potential of the nonlinear endstate (defined as $t = [150 : 300]\ L_n/C_s$) is extremely well-predicted by the analytic form presented by Hasegawa and Wakatani [26], based on the conservation of angular momentum and energy; the only difference is that the mean zonal potentials and flows are of almost exactly equal but opposite magnitude in the two simulation cases. The zonal potentials are for both cases plotted in figure 7; the dashed lines represent the Hasegawa–Wakatani prediction, normalized to the potentials at $r = 0$. As described above, in both cases the zonal potentials are set equal to zero as initial conditions, so

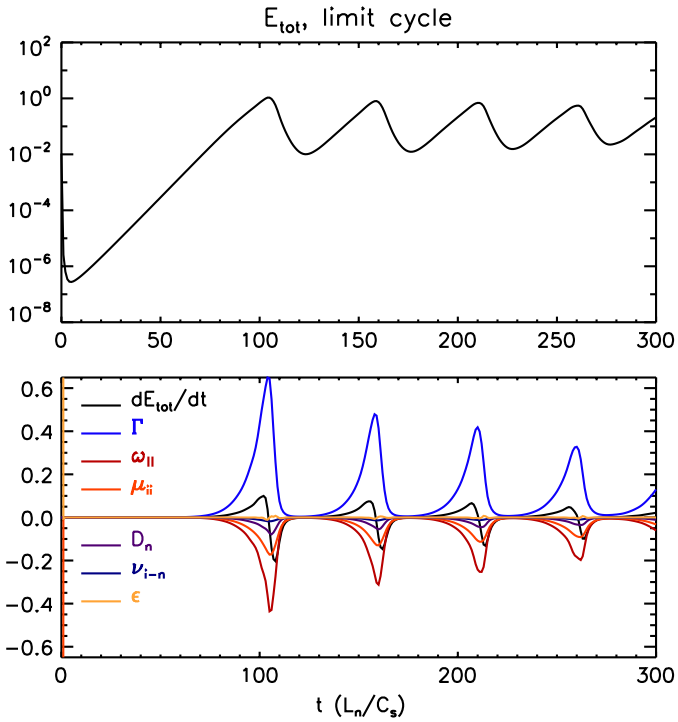

Figure 3. Time trace of E_{tot} and various terms of energy balance equation for the limit cycle case.

that both simulations are initialized with zero net angular momentum $M = \int\int \mathrm{d}^2 r r V_\theta$, just as in the original work by Hasegawa and Wakatani.

Because the two cases were found with the same physical and numerical parameters, it appears that the final state reached must depend sensitively on the initial distribution of phases of the initial fluctuations. To rule out the influence of numerical effects, two tests were undertaken. First, the two cases were rerun using the exact same initial conditions (i.e. including initial phase distributions), but using a time step $\Delta t = 2.5 \times 10^{-3}\ L_{\mathrm{n}}/C_{\mathrm{s}}$ (i.e. half of the original value); in both cases the dynamics were exactly reproduced. Second, both simulations were run for additional 300 $L_{\mathrm{n}}/C_{\mathrm{s}}$, but with the signs of the zonal flows reversed. Reversing the sign of the zonal flow caused the turbulence to transition from one state to the other, i.e. from the limit cycle to the steady case, and vice versa. Reversing the sign not only caused the system to transition, but caused the dominant m number of the fluctuations to change accordingly as well—to go from $m = 2$ dominant in the steady case to $m = 3$ dominated in the limit cycle case and from $m = 3$ to 2 dominant in the reverse transition. Alternatively, reversing the sign of the finite m fluctuations but not the zonal flow did not cause the system to change states (consistent with expectations from equations (1) and (2) if zonal flow convection of the finite m fluctuations is dominant). The effects of reversing the signs of the zonal flow and finte m fluctuations are shown in figure 8. Given the robustness of the nonlinear states to the timestep used, the excellent energy conservation and the formation of a self-organized zonal flow in excellent agreement with an analytic prediction based upon conserved quantities of the computational model, both states appear to be physically meaningful and determined sensitively by the initial conditions. Although the linear phases of the two states appear to be quite similar, close examination suggests the limit cycle case has slightly more power in the

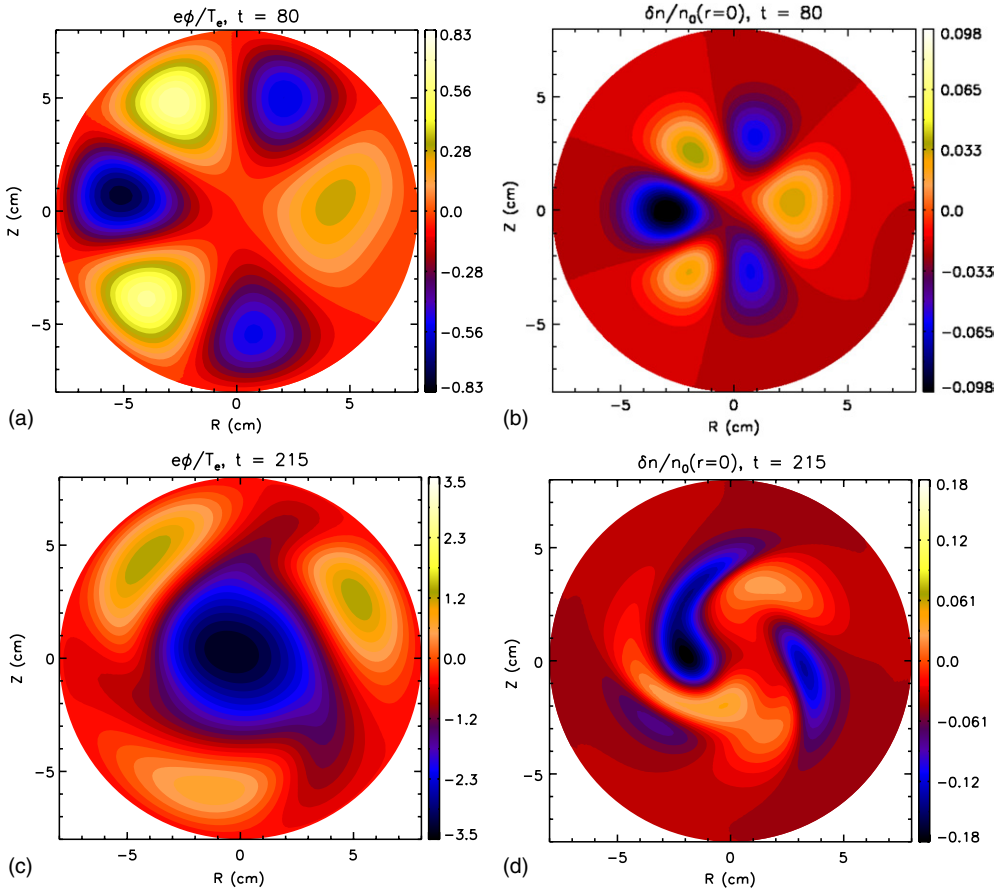

Figure 4. Snapshots of the potential density during the linear ($t = 80$) and nonlinear ($t = 210$) phases of the limit cycle case.

odd $m = 1$ and 3 modes than in the even $m = 2$ and 4 modes, while the steady case exhibited the reverse; these initial conditions clearly correlate with the final state. The robustness of the two states and the finite number of poloidal (and radial) modes involved suggest that a probabilistic approach might be able to predict the final state. A reduced set of equations for the amplitude and phases of the zonal and first and second radial modes associated with $m = 3$ and 4 could be constructed and the existence of two attractors corresponding to two nonlinear states searched for.

4. Comparison to experimental profiles

While the simulations described above represent an interesting limit for the investigation of zonal flow dynamics in and of themselves, determining how well they predict actual experimental profiles is ultimately the most important test. As described in previous papers (and shown in figure 1), there was relatively good qualitative agreement between the mean zonal flow predicted by the limit cycle simulation results and the published experimental results. Conversely, the zonal flow predicted by the new steady state simulations reproduces the spatial

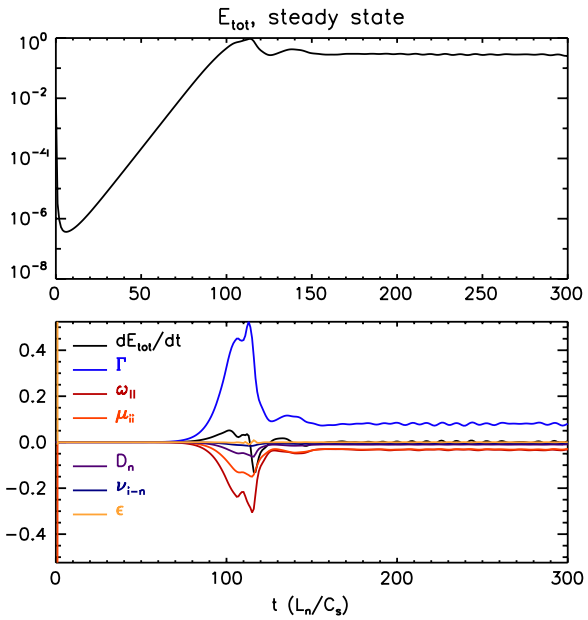

Figure 5. Time trace of $E_{\rm tot}$ and various terms of energy balance equation for a simulation which enters the steady nonlinear endstate.

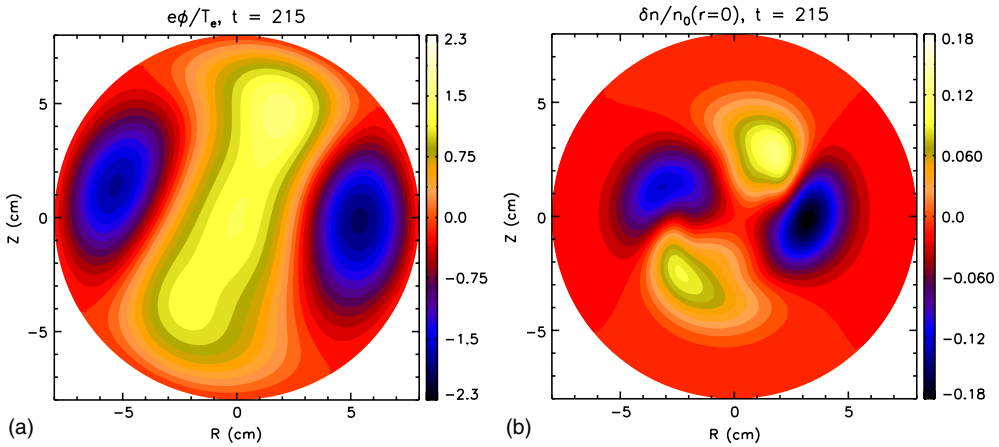

Figure 6. Snapshots of the potential and density during the nonlinear phase ($t = 210$) of the nonlinear state.

profile of the measured zonal flow equally well but is in the wrong direction (i.e. the simulation zonal flow is in the ion diamagnetic direction, while the experiment indicates flow in the electron diamagnetic direction). Comparisons of the experimentally measured profiles of mean density and root mean square (RMS) density and potential fluctuations against the simulation results are shown in figure 9. While there is fair agreement with the density fluctuation profile, the magnitude of the density fluctuations is overestimated for both cases. However, there is more than an order of magnitude difference in the peak values of the experimental measured floating potential fluctuations and plasma potential fluctuations from the simulation.

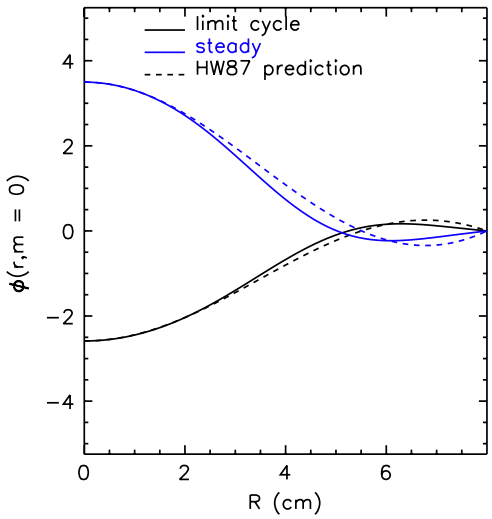

Figure 7. Mean zonal potentials from both simulation cases, averaged over $t = [150 : 300]$. The solid curves are the simulation results, while the corresponding dashed curves are the analytically predicted profile of Hasegawa and Wakatani, normalized to the simulation potential at $r = 0$. The limit cycle curve is negative at $r = 0$, while the steady curve is positive.

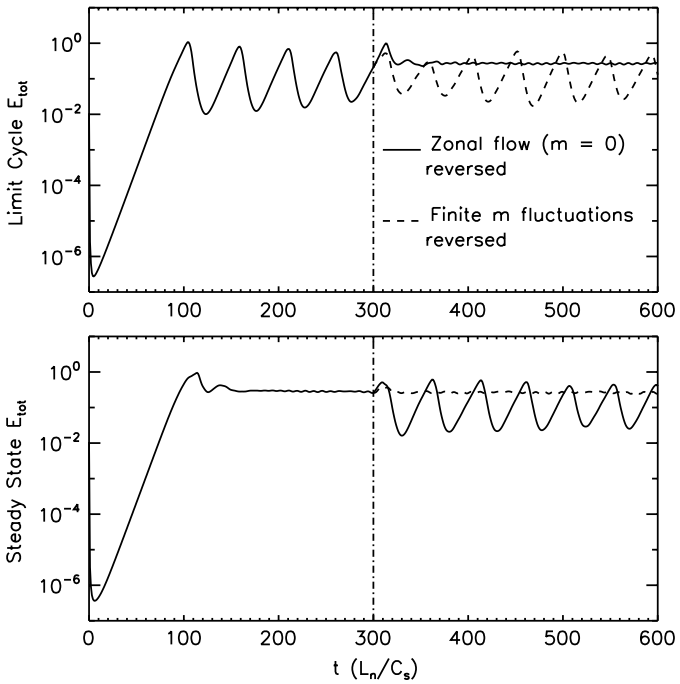

Figure 8. Time traces of $E_{\rm tot}$ in the cases for which the sign of the zonal flow sign is reversed at $t = 300$ (solid lines), and the finite m fluctuations are reversed (dashed curves), demonstrating that changing the sign of the zonal flow induces a transition to the other endstate, but changing the sign of the fluctuations does not. The vertical dashed–dotted lines indicate the transition point at $t = 300$.

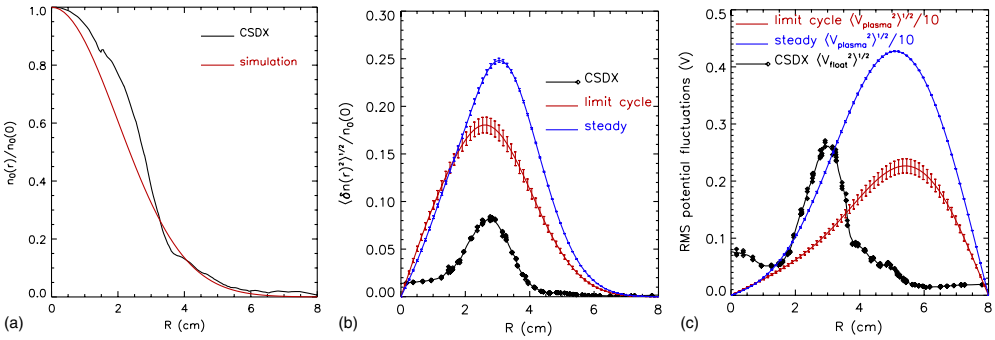

Figure 9. Comparison of simulation results with experiment. (*a*) Experimentally measured mean density profile and Gaussian profile used in simulation. RMS density fluctuations (*b*) and potential fluctuations (*c*) measured in CSDX, compared against limit cycle and steady state results.

One potential source of the disagreement in the potential fluctuations is that while there is a straightforward procedure for translating the ion saturation current measured via a Langmuir probe into electron density, the connection between the floating potential measured by the probe and the plasma potential described by the simulation is much more complex, as it is strongly influenced by electron temperature fluctuations due to the effect of the sheath surrounding the probe tip [27]. A second, more fundamental point of disagreement between the simulations and experiment is that while no strong coherent limit cycle is observed in the experiment, the outer region ($r > 4$ cm) is observed to be highly bursty and intermittent, which is not observed in the simulation. Work by a number of groups [28–30] has shown that when the 'equilibrium' components of the density and temperature gradients (i.e. the $m = 0$ density component in our simulation) which drive the turbulence are allowed to self-consistently evolve in response to the instantaneous turbulent flux rather than being held fixed (as n_0 currently is in our simulation), a large variety of intermittent behaviour which would otherwise be missed is observed. Other potential sources of discrepancy are the assumption of a single, fixed value of $k_\parallel$ for all the finite m modes (and $k_\parallel = 0$ for the zonal potential), parallel boundary conditions, the neglect of temperature fluctuations and the effects of 'nonlocality' (i.e. finite ρ_s/L_n). We plan to extend the model to include such effects (beginning with a source driven density and multiple values of $k_\parallel$) and will report on them in a future publication. For now, one can say that using the simplest model of drift-wave turbulence which includes a self-consistent linear instability and turbulent flux, some of the general features of a corresponding experimental realization can be qualitatively reproduced (e.g. the formation of a system-scale zonal flow and density fluctuations peaked near the peak mean density gradient) but that quantitative predictions remain quite difficult.

Acknowledgments

The authors wish to thank P H Diamond, S-I Itoh, K Itoh, S Muller and F Spineanu for many valuable suggestions and conversations. Discussions with S-I Itoh, K Itoh, and F Spineanu were made possible by the Grant-in-Aid for Specially-Promoted Research of MEXT Japan (16002005). This research was performed under grants DE-FG02-04ER54773 and DE-FG02-04ER54734. C H performed this research under an appointment to the Fusion Energy Postdoctoral Research Program, administered by the Oak Ridge Institute for Science

and Education under contract number DE-AC05-00OR22750 between the US Department of Energy and Oak Ridge Associated Universities.

References

[1] Horton W 1999 *Rev. Mod. Phys.* **71** 735
[2] Terry P W 1999 *Rev. Mod. Phys.* **72** 109
[3] Diamond P H and Kim Y B 1991 *Phys. Fluids* B **3** 1626
[4] Biglari H, Diamond P H and Terry P W 1990 *Phys. Fluids* B **2** 1
[5] McKee G R *et al* 2003 *Phys. Plasmas* **10** 1712
[6] Fujisawa A *et al* 2004 *Phys. Rev. Lett.* **93** 165002
[7] Conway G D *et al* 2005 *Plasma Phys. Control. Fusion* **47** 1165
[8] Nagashima Y *et al* 2005 *Phys. Rev. Lett.* **95** 095002
[9] Shats M G, Xia H and Punzmann H 2005 *Phys. Rev.* E **71** 046409
[10] Sen A K, Sokolov V and Wei X 2006 *Phys. Plasma* **13** 055905
[11] 2006 *Plasma Phys. Control. Fusion* **48** S1–S212 (a special issue on experimental studies of zonal flows and turbulence)
[12] Diamond P H, Itoh S I, Itoh K and Hahm T S 2005 *Plasma Phys. Control. Fusion* **47** R35
[13] Kraichnan T H 1967 *Phys. Fluids* **10** 1417
[14] Burin M, Antar G, Crocker N, Tynan G R 2005 *Phys. Plasmas* **12** 052320
[15] Tynan G R *et al* 2004 *Phys. Plasmas* **11** 5195
[16] Tynan G R *et al* 2006 *Plasma Phys. Control. Fusion* **48** S51
[17] Holland C *et al* 2006 *Phys. Rev. Lett.* **96** 195002
[18] Holland C *et al* 2004 *Rev. Sci. Instrum.* **75** 4278
[19] Hasegawa A and Wakatani M 1983 *Phys. Rev. Lett.* **50** 682
[20] Hasegawa A and Mima K 1978 *Phys. Fluids* **21** 87
[21] Gondarenko N A and Guzdar P N 1999 *Geophys. Res. Lett.* **26** 3345
[22] Hassam A B and Antonsen T M Jr 1994 *Phys. Plasmas* **1** 337
[23] Burrell K H 1997 *Phys. Plasmas* **4** 1499
[24] Arakawa A 1966 *J. Comput. Phys.* **1** 119
[25] Diamond P H *et al* 1998 *Proc. 17th IAEA Fusion Energy Conf. (Yokohama, Japan)* (Vienna: IAEA) CD-ROM file TH3/1 and http://www.iaea.org/programmes/ripc/physics/start.htm
[26] Hasegawa A and Wakatani M 1987 *Phys. Rev. Lett.* **59** 1581
[27] See R A Moyer *et al* 1995 *Phys. Plasmas* **2** 2397 (appendix A)
[28] Naulin V, Juul Rasmussen J and Nycander J 2003 *Phys. Plasmas* **10** 1075
[29] Garcia O E, Naulin V, Nielsen A H and Juul Rasmussen J 2005 *Phys. Plasmas* **12** 062309
[30] Beyer P *et al* 2005 *Phys. Rev. Lett.* **94** 105001